Noninvasive Molecular Ultrasound Monitoring of Vessel Healing After Intravascular Surgical Procedures in a Preclinical Setup

Adelina Curaj,* Zhuojun Wu,* Stanley Fokong, Elisa A. Liehn, Christian Weber, Alexandrina Burlacu, Twan Lammers, Marc van Zandvoort, Fabian Kiessling

Objective—Cardiovascular interventions induce damage to the vessel wall making antithrombotic therapy inevitable until complete endothelial recovery. Without a method to accurately determine the endothelial status, many patients undergo prolonged anticoagulation therapy, denying them any invasive medical procedures, such as surgical operations and dental interventions. Therefore, we aim to introduce molecular ultrasound imaging of the vascular cell adhesion molecule (VCAM)-1 using targeted poly-*n*-butylcyanoacrylate microbubbles (MB_{VCAM-1}) as an easy accessible method to monitor accurately the reendothelialization of vessels.

Approach and Results—*ApoE*$^{-/-}$ mice were fed with an atherogenic diet for 1 and 12 weeks and subsequently, endothelial denudation was performed in the carotid arteries using a guidewire. Molecular ultrasound imaging was performed at different time points after denudation (1, 3, 7, and 14 days). An increased MB_{VCAM-1} binding after 1 day, a peak after 3 days, and a decrease after 7 days was found. After 12 weeks of diet, MB_{VCAM-1} binding also peaked after 3 days but remained high until 7 days, indicating a delay in endothelial recovery. Two-photon laser scanning microscopy imaging of double fluorescence staining confirmed the exposure of VCAM-1 on the superficial layer after arterial injury only during the healing phase. After complete reendothelialization, VCAM-1 expression persisted in the subendothelial layer but was not reachable for the MB_{VCAM-1} anymore.

Conclusion—Molecular ultrasound imaging with MB_{VCAM-1} is promising to assess vascular damage and to monitor endothelial recovery after arterial interventions. Thus, it may become an important diagnostic tool supporting the development of adequate therapeutic strategies to personalize anticoagulant and anti-inflammatory therapy after cardiovascular intervention. (***Arterioscler Thromb Vasc Biol*. 2015;35:1366-1373. DOI: 10.1161/ATVBAHA.114.304857.)**

Key Words: atherosclerosis ■ microbubbles ■ molecular imaging ■ ultrasonography

Restenosis and in-stent thrombosis after revascularization procedures are major obstacles in the local treatment of atherosclerotic plaques.[1,2] It has been shown that an intact endothelial layer has antithrombotic and atheroprotective properties,[3] acting as a barrier against lipid uptake and inflammatory cell recruitment.[4] Even though drug-eluting stents reduce restenosis through the suppression of vascular smooth muscle cell (VSMC) proliferation and migration,[5,6] complications such as in-stent thrombosis are still notable events[7,8] because of delayed endothelial recovery.

See cover image

The regrowth of the endothelium downregulates intimal smooth muscle cell proliferation, retards plaque development,[4,9] and consequently reduces the risk for postinterventional complications. Therefore, the monitoring of vascular restoration is important in therapeutic postinterventional follow-up. Suitable markers for monitoring vascular damage should ideally be expressed immediately after arterial denudation, and should remain to be expressed until reendothelialization is complete.

Received on: October 21, 2014; final version accepted on: March 22, 2015.

From the Institute for Experimental Molecular Imaging (A.C., Z.W., S.F., T.L., F.K.), Institute for Molecular Cardiovascular Research (A.C., Z.W., E.A.L., M.v.Z.), University Clinic, RWTH Aachen University, Aachen, Germany; Institute of Cardiovascular Prevention, Ludwig-Maximilians-University Munich, Munich, Germany (C.W.); DZHK (German Centre for Cardiovascular Research, partner site Munich Heart Alliance), Munich, Germany (C.W.); Institute of Cellular Biology and Pathology "Nicolae Simionescu" of the Romanian Academy, Bucharest, Romania (A.B.); Department of Controlled Drug Delivery, University of Twente, AE Enschede, The Netherlands (T.L.); and Department of Genetics and Molecular Cell Biology, School for Cardiovascular Diseases CARIM, Maastricht University, Maastricht, The Netherlands (M.v.Z.).

*These authors contributed equally to this article.

This manuscript was sent to Ryozo Nagai, Consulting Editor, for review by expert referees, editorial decision, and final disposition.

The online-only Data Supplement is available with this article at http://atvb.ahajournals.org/lookup/suppl/doi:10.1161/ATVBAHA.114.304857/-/DC1.

Correspondence to Fabian Kiessling, MD, Institute for Experimental Molecular Imaging, University Clinic, RWTH Aachen University, Pauwelsstrasse 30, 52074 Aachen, Germany. E-mail fkiessling@ukaachen.de; or Marc van Zandvoort, PhD, Department of Genetics and Molecular Cell Biology, School for Cardiovascular Diseases CARIM, Maastricht University, P. Debyelaan 25, 6229 HX Maastricht, The Netherlands. E-mail mamj.vanzandvoort@maastrichtuniversity.nl

Nonstandard Abbreviations and Acronyms	
ECs	endothelial cells
MBs	microbubbles
MB_{CTR}	microbubbles control
MB_{VCAM-1}	VCAM-1–targeted microbubbles
PECAM-1	platelet/EC adhesion molecule 1
TPLSM	two-photon laser scanning microscopy
VCAM-1	vascular cell adhesion molecule-1
VSMCs	vascular smooth muscle cells

Consequently, such markers have to be expressed on both, the VSMCs (being exposed to the blood after endothelial removal) and the activated, regenerating endothelial cells (ECs), which start covering the vascular wound (Figure I in the online-only Data Supplement). Finally, the markers should show a low luminal exposure under physiological conditions.

Ultrasound imaging using targeted microbubbles (MBs) can potentially provide valuable insights into the presence of prominent inflammation surface markers during the various states of endothelial regeneration, allowing the personalization of anti-inflammatory therapy in dosage, medication period, and combination.

In this study, we propose vascular cell adhesion molecule (VCAM)-1 as an ultrasound imaging biomarker of endothelial healing in big vessels, such as carotid arteries. VCAM-1 is expressed by activated VSMCs and it is accessible for intravascular targeting after arterial denudation, whereas replicating ECs express VCAM-1 during endothelial reconstruction until regeneration[10,11] (Figure I in the online-only Data Supplement). We, therefore, used VCAM-1–targeted MBs (MB_{VCAM-1}) and molecular ultrasound to monitor arterial endothelial recovery, and validated the results using two-photon laser scanning microscopy (TPLSM) as a deep-tissue imaging modality. TPLSM was applied for the characterization of VCAM-1 expression, MB binding, and morphological changes in the arterial lumen on cellular and subcellular levels. Our data provide strong evidence that MB_{VCAM-1} are suitable for noninvasive molecular ultrasound monitoring of vascular healing in a murine model of endothelial denudation.

Materials and Methods

Materials and Methods are available in the online-only Data Supplement.

Results

Ex Vivo Whole Mount Artery TPLSM Imaging of Wire-Injured Carotids

Before endothelial denudation, animals were fed a high cholesterol diet for either 1 week (short-term diet) or 12 weeks (long-term diet). The majority of experiments were conducted on animals with a short-term diet to induce hyperlipidemia, to validate MB_{VCAM-1}–binding specificity and efficiency under postinterventional conditions. The long-term diet group was

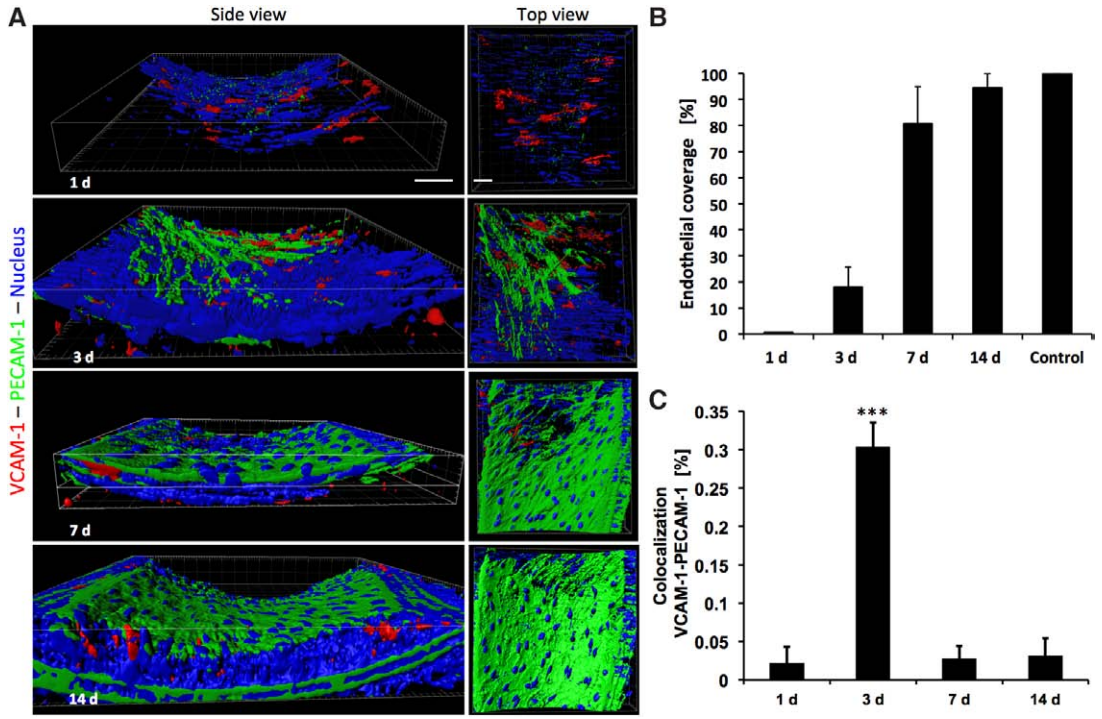

Figure 1. Three-dimensional rendering of denudated carotid arteries of mice from the short-term atherogenic diet group and quantification of endothelial recovery. Using platelet/endothelial cell adhesion molecule (PECAM)-1 as a marker for endothelial cells and vascular cell adhesion molecule (VCAM)-1 for endothelial regeneration, z-stack images were rendered to better illustrate the extent of regeneration and inflammation. **A**, The degree of endothelial regeneration is depicted starting from 1 day until 14 days post denudation. **B**, Graph reporting the percentage of endothelial coverage in carotid arteries before and after denudation, compared with control vessels. While directly after denudation, almost the entire vessel surface was removed, 94% of the endothelial surface coverage was reconstituted after 14 days. **C**, To illustrate the availability of endothelial VCAM-1, the Manders coefficient for VCAM-1 colocalization with PECAM-1 for all time points was calculated. Scale bar, 25 μm.

introduced to investigate the effect of high cholesterol diet on the rate of endothelial regeneration after plaque removal by wire injury and the potential of molecular ultrasound to distinguish between both the conditions.

First, the VCAM-1 expression pattern and the degree of endothelial regeneration were studied in mice on short-term diet after endothelial denudation. We stained ex vivo mounted carotid arteries for platelet/EC adhesion molecule (PECAM)-1, VCAM-1, and nuclei, and analyzed marker expression using TPLSM at the 4 different time points (1, 3, 7, and 14 days: Figure 1A; Figure II in the online-only Data Supplement). Three-dimensional (3D) reconstruction of the vessel wall and quantification of the endothelial regeneration showed only EC debris at 1 day, and an endothelial coverage of 18% after 3 days, 80% after 7 days, and 94% after 14 days, respectively (Figure 1B).

The EC debris at day 1 was positive for VCAM-1 (Figure II in the online-only Data Supplement). At this time point, VCAM-1 was found to be highly expressed on VSMCs as well. The first signs of endothelial regeneration were visible 3 days after denudation, in conjunction with the highest colocalization of VCAM-1 with the endothelial marker PECAM-1, indicating pronounced ECs activation and regeneration (Figure 1C). In parallel, the VSMCs exposed to the vascular lumen also displayed a strong VCAM-1 expression. At later time points (7 and 14 days), ECs regeneration progressed further, showing a continuous decrease in VCAM-1 expression down to the level of noninjured controls after 14 days (Figure 1A; Figure II in the online-only Data Supplement). In contrast, VCAM-1 expression on VSMCs remained high even 14 days after denudation, however, these VSMCs were not luminally exposed anymore and thus not accessible to MB_{VCAM-1}. These findings are in line with the mean fluorescence intensity quantifications for VCAM-1 and PECAM-1 expression (Figure III in the online-only Data Supplement).

Ultrasound Analysis of MB_{VCAM-1} Binding to Carotid Arteries After Wire Injury in a Flow Chamber

MB_{VCAM-1} binding to carotid arteries was studied in mice from the short-term diet group, 1 day after endothelial denudation. First, the efficiency and specificity of MB_{VCAM-1} binding to VCAM-1 under flow conditions in early denudated carotid arteries was investigated ex vivo. Approximately 9-fold higher signal decrease after MB_{VCAM-1} destruction in denudated carotid arteries compared with the control carotid arteries was found ($P<0.001$). In addition, ≈8-fold higher signal decrease after MBs destruction was obtained in denudated carotid arteries when compared with the competitive-binding group, as well as to nontargeted MBs ($P<0.05$ and $P<0.05$, respectively) indicating strong binding of MB_{VCAM-1} to its target (Figure 2).

TPLSM Analysis of MB_{VCAM-1}–Binding Specificity to Carotid Arteries After Wire Injury in a Flow Chamber

Next, the extent and specificity of rhodamine-labeled MB_{VCAM-1} binding was validated in flow-chamber experiments using TPLSM (Figure 3A). Three days after endothelial denudation, carotid arteries of mice from the short-term diet group were excised and perfused under physiological flow rates (0.5 mL/min) with MB_{VCAM-1}. After MBs' binding and washing, the carotid arteries were stained for VCAM-1, PECAM-1,

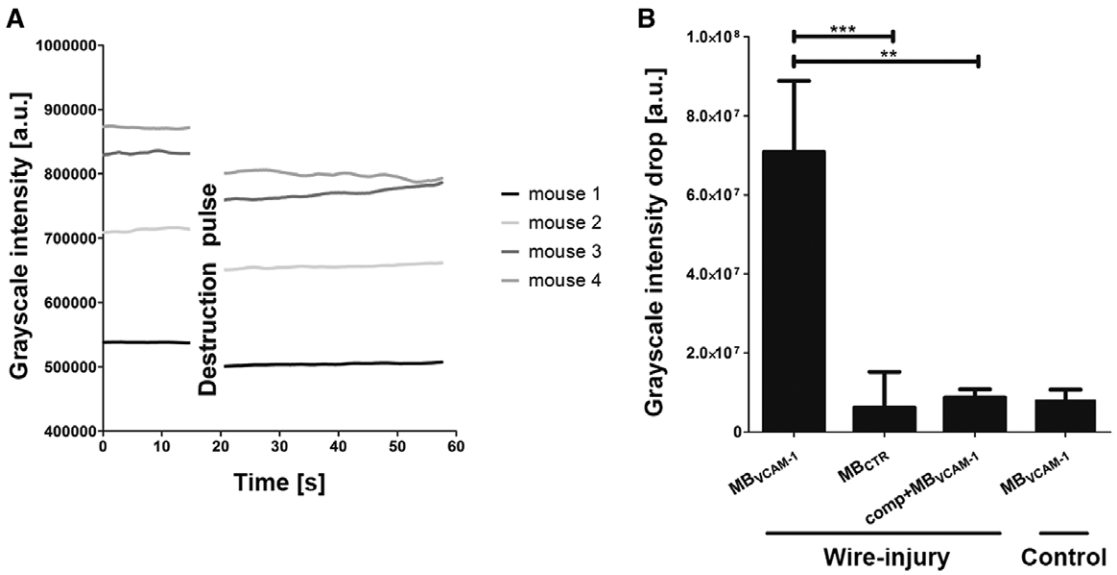

Figure 2. Ex vivo molecular ultrasound imaging of denudated carotid arteries of mice from short-term atherogenic diet group. To investigate the specificity of MB_{VCAM-1} binding to vascular cell adhesion molecule (VCAM)-1 in early denudated carotid arteries and to evaluate the potential in vivo application of the imaging method, ex vivo measurements were performed first. **A**, Example of a MB_{VCAM-1} destruction/replenishment curves (n=4) recorded in flow-chamber experiments. Common carotid arteries were excised and mounted in a customized flow chamber. At time point 0, the mixture of MB_{VCAM-1} and blood, which had been circulating for 10 minutes was removed and replaced with Hanks' balanced salt solution for imaging. **B**, Quantification and statistical analysis of MB binding (n=4 mice per group; total of 12 animals) showing a significantly higher binding of MB_{VCAM-1} to 1 day denudated carotid arteries compared with control carotids, as well as a significantly higher binding of MB_{VCAM-1} to 1 day denudated carotid arteries compared with both, MB_{CTR} and to the competitive-binding group where carotid arteries were incubated with 20-fold higher concentration of free anti-CD106 antibody. CTR indicates control; and MB, microbubbles.

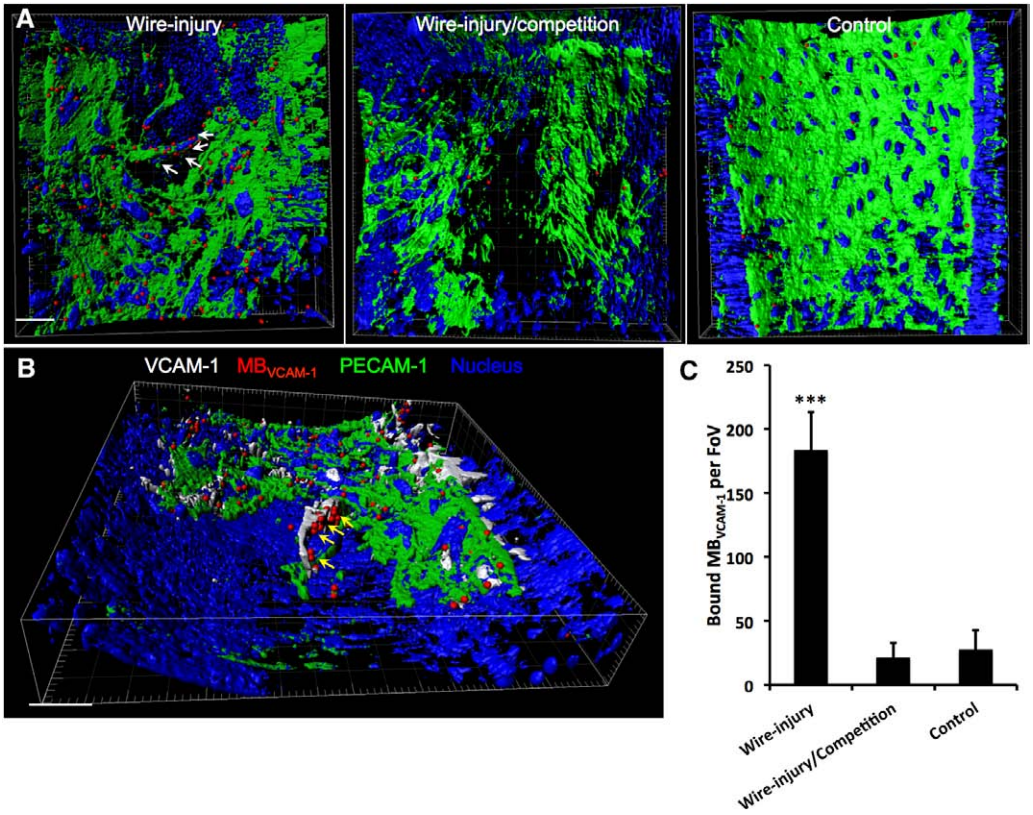

Figure 3. Ex vivo two-photon laser scanning microscopy flow-chamber images of carotid arteries 3 days post endothelial denudation and of control arteries of mice from short-term atherogenic diet group. For validation of vascular cell adhesion molecule (VCAM)-1 as a molecular target under flow, MB_{VCAM-1} was flowed on denudated and control vessels. **A**, Rhodamine-labeled MB_{VCAM-1} strongly bind in denudated carotid arteries (white arrows) but hardly in control ones, as well as denudated ones on competitive binding with excess-free VCAM-1 antibody. **B**, Costaining of platelet/endothelial cell adhesion molecule (PECAM)-1, VCAM-1, and nuclei after MB_{VCAM-1} perfusion of denudated carotid arteries shows colocalization of MB_{VCAM-1} with VCAM-1 staining (yellow arrows). **C**, Graph showing the results of the quantitative analysis of MB_{VCAM-1} binding. In comparison to experiments with MB_{VCAM-1}, only a significantly lower binding in the presence of competing antibodies was found in denudated and control arteries. Scale bar, 50 μm. HFD indicates high cholesterol diet; and MB, microbubbles.

and nuclei, showing bound MBs to be colocalized with the VCAM-1 signal. MB_{VCAM-1} binding to the denudated artery was ≈7-fold higher compared with the control artery. Under competitive-binding conditions, MB_{VCAM-1} accumulation was suppressed by a factor of ≈9 (Figure 3C).

In vivo Evaluation of MB_{VCAM-1} Binding to VCAM-1 Using Ultrasound and TPLSM

Finally, MB_{VCAM-1} binding and detection was validated in vivo. First, in vivo MB_{VCAM-1} binding was tested 1 day after endothelial denudation in mice from the short-term diet group. Using contrast mode, the MBs influx after injection could be visualized (Figure 4A) and quantified (Figure 4B). After clearance of circulating MB_{VCAM-1}, bound MB_{VCAM-1} were found attached to the inner vessel wall (Figure 4A). Binding of significant amounts of MB_{VCAM-1} was further confirmed by a strong drop in ultrasound signal intensity after the application of a destruction pulse (Figure 4C). Competitive-binding experiments showed the specificity of MB_{VCAM-1} to its intended target at day 1 postsurgery in denudated carotid arteries: after blocking VCAM-1 with excess-free antibody before MB_{VCAM-1} injection, there was a drop in MB_{VCAM-1}–specific signals by 90 (±8) % (Figure 4D).

To verify MB binding, we performed in vivo TPLSM measurements with rhodamine-loaded[12–14] MB_{VCAM-1} in wire-injured carotids. After creating a surgical window for TPLSM,[15] we tracked single-bound MBs in a field of view of 500×500 μm. Immediately after injection, we monitored the influx of circulating MBs (Figure IVA in the online-only Data Supplement), which was followed by a rapid clearance within ≈5 minutes. Although nontargeted and targeted MBs under competitive-binding conditions with free VCAM-1 antibodies did not significantly bind to the vascular wall of denudated carotid arteries (3 days after denudation), many stationary MB_{VCAM-1} were detected at the luminal side of the carotid artery for >6 minutes (Figure IVB in the online-only Data Supplement). Even after euthanasia, excision and mounting of the carotid arteries, MB_{VCAM-1} were still present within the lumen (Movie I in the online-only Data Supplement).

Comparative Ultrasound Imaging Using MB_{VCAM-1} to Assess Endothelial Regeneration in Mice on Short- and Long-Term Atherogenic Diet In Vivo

A short-term diet of 1 week before denudation only induces hyperlipidemia without plaque development. In contrary,

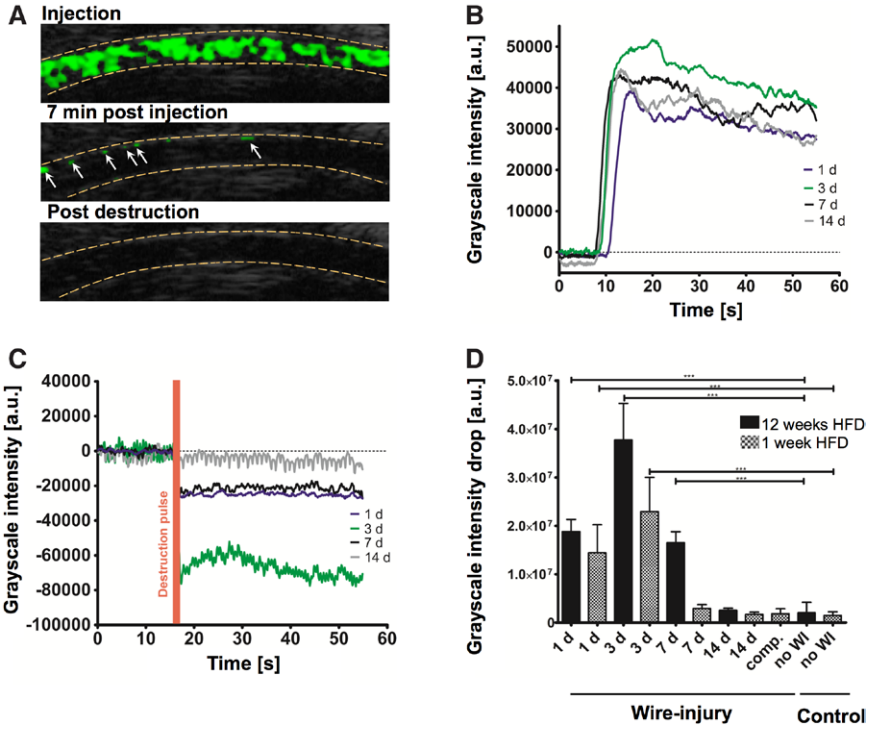

Figure 4. In vivo molecular ultrasound (US) imaging of denudated carotid arteries. US monitoring of endothelial recovery in vivo was performed using the destruction-replenishment curve of injected MB_{VCAM-1}. **A**, Representative results from in vivo contrast mode molecular US imaging of murine carotid arteries in a long-axis imaging plane showing (**top**) the contrast mode US image of circulating MB_{VCAM-1} in the blood; **middle**, US image before the destructive pulse showing MB_{VCAM-1} bound to their target; **bottom**, US image after MB_{VCAM-1} destruction displaying a microbubble (MB)-free lumen. MBs are color-coded in green; stationary MBs are indicated with white arrows. **B**, The normalized in vivo MB injection curve shows an increase in grayscale intensity concomitantly with the inflow of the MBs. C, Examples of normalized MB_{VCAM-1} destruction-replenishment sequences for each time point after endothelial denudation (1, 3, 7, and 14 days) in mice from long-term diet. Circulation time of MB_{VCAM-1} before the destructive pulse was 7 minutes. **D**, The quantification and statistical analysis of MB binding (n=4–5 animals per group) indicates specific binding of MB_{VCAM-1} to denudated carotid arteries (short-term high cholesterol diet—chess pattern bars, long-term high cholesterol diet—solid bars). Competitive-binding experiments were conducted in a separate group of animals (also 1 day after arterial injury), confirming specific MB_{VCAM-1} binding. PECAM indicates platelet/endothelial cell adhesion molecule; and VCAM indicates vascular cell adhesion molecule.

a long-term diet (12 weeks) leads to signs of early plaque growth. Thus, it was of interest to confirm that our molecular ultrasound approach was capable to assess vascular regeneration in both cases and to compare the course of healing. A significantly enhanced binding of MB_{VCAM-1} in carotid arteries could only be observed at early time points after endothelial denudation, starting immediately (1 day) and peaking at 3 days (Figure 4D) in both short- and long-term diet groups. In the short-term diet group, quantification showed ≈8-fold increase in ultrasound grayscale intensity difference after 1 day, and ≈15-fold increase after 3 days, compared with the control group (P<0.001 and P<0.001, respectively), whereas at day 7, only a 2-fold increase in ultrasound grayscale intensity difference compared with the control group (P>0.05) was measured. At early time points, similar results were obtained in the long-term diet group, presenting ≈9-fold increase in ultrasound grayscale intensity difference after 1 day, and ≈18-fold increase after 3 days, (P<0.05 and P<0.001, respectively). However, after 7 days still a ≈8-fold increase (P<0.001) was found in the long-term diet group, indicating a delayed endothelial recovery after wire injury, which translated into a prolonged VCAM-1 availability detected by ultrasound through MB_{VCAM-1} binding. Fourteen days post surgery, MB_{VCAM-1} binding dropped down to the level of unhandled control animals in both short- and long-term diet groups, showing that endothelial recovery can be monitored by ultrasound molecular imaging.

Immunohistology of Denudated Arteries From Long-Term Diet Group

Finally, we validated reendothelialization and VCAM-1 expression in the carotid arteries of the long-term diet group by immunohistology at 1, 3, 7, and 14 days after denudation (Figure V in the online-only Data Supplement). In control carotid arteries, VCAM-1 was found in small spots at the endothelial surface (<3% of the total area), where native plaques were developing. One day after denudation, endothelial CD31 was absent, whereas VCAM-1 was present at the luminal side and in the media. Three and 7 days after denudation, both CD31 and VCAM-1 were visible at the luminal side of the artery, whereas after 14 days VCAM-1 was only detected in the media or under the CD31-stained intima.

Discussion

The endothelial response to interventional procedures after blood flow restoration in atherosclerotic arteries is one of the most important factors determining patient recovery. The degree of endothelial damage correlates to the risk of

neointima growth, platelet adhesion, and thrombosis. Thus, it precludes the success of interventional surgery, that is, slower endothelial regeneration causing a higher risk for complications.[7] After the intervention, dual antiplatelet medication and inflammatory inhibitors are applied using a standardized dosage, medication period, and combination, which is independent of the recovery rate of individual patients. However, the patient's age, general immune state, comorbidities, such as diabetes mellitus, and the different size of the plaque and injured area can strongly influence the speed of regeneration and degree of inflammation.[16,17] Thus, there seems to be a clear need for a reliable diagnostic assessment of endothelial regeneration, as well as for the individualization of postinterventional anticoagulant and anti-inflammatory therapy.

For this purpose, as a cheap and real-time imaging modality with excellent spatial resolution, molecularly targeted ultrasound imaging may be the modality of choice. However, the selection of the target for the molecular probe must be done carefully and the target should fulfil 3 criteria, such as (1) subendothelial expression after endothelial denudation (eg, expression by luminally exposed VSMCs); (2) expression by the activated regenerating ECs; and (3) absence/low constitutive expression after reendothelialization. Previous studies have shown results indicating that some markers may have a constitutive expression level (PECAM-1, ICAM-1, P-selectin, and E-selectin),[11,14,18–20] other markers might either be not sufficiently expressed on activated VSMCs (PECAM-1, E-selectin, and P-selectin),[18,21,22] or remain to be upregulated for a prolonged period of time after complete structural recovery (PECAM-1 and ICAM-1)[19] (Table I; Figure VI in the online-only Data Supplement).

On the basis of the current literature, VCAM-1 was chosen in this study as a target for several reasons: VCAM-1 is one of the most well-known atherosclerotic markers.[23] It has already been used for visualizing aortic atherosclerotic lesions by molecular ultrasound.[24–26] Despite its major application in atherosclerosis, VCAM-1 is also an acute inflammatory marker that is highly expressed after vascular injury, and it plays a major role in the formation of neointima and restenosis.[27] It was previously described that VCAM-1 is expressed by both ECs[28] and VSMCs[29,30] in atherosclerotic arteries. However, binding of MB_{VCAM-1} to VCAM-1 is dependent on its luminal availability. On the basis of immunofluorescence quantifications and 3D renderings of the vessels, 1 day after endothelial denudation, activated medial VSMCs expressing VCAM-1 are exposed to the blood flow, presenting the only source for MB_{VCAM-1} binding because ECs were removed by endothelial denudation. Three days after denudation, the endothelial layer is regenerating. The activated and proliferating ECs express VCAM-1 as well, presenting an additional source for VCAM-1. Consequently, MB binding peaks because of higher receptor availability. Subsequently, VCAM-1 expression by ECs decreases with endothelial regeneration. Therefore, significant colocalization of VCAM-1 with PECAM-1 could only be observed at 3 days because of the lack of ECs after 1 day, and the absence of endothelial activation after 14 days, when endothelial coverage was close to complete. After endothelial recovery subendothelial and intimal markers, even though present and upregulated (Figure I and II in the online-only Data Supplement), are not accessible to MBs anymore. The lack of MB_{VCAM-1} binding then indicates completion of the endothelial regeneration and the return of ECs toward a physiological state. Mice fed for 14 weeks with atherogenic diet showed a delay in endothelial recovery. This is not surprising because high cholesterol diet and obesity-related pathologies, such as diabetes mellitus have been reported to interfere and delay wound healing and prolong the inflammatory phase, both in animals and in patients.[31–33] Even though VCAM-1 was upregulated in the early plaque region of the control artery, significant MB_{VCAM-1} binding in mice with 12 weeks of diet was not detected. A possible explanation could be the limited size of the plaque area, comprising only 3% of the total endothelial surface (data not shown), which may not be sufficient to induce visible MB binding above the background noise level.

Previously, ultrasound imaging was used for the noninvasive visualization of typical in-stent restenosis after carotid stenting of the internal carotid artery in humans.[34–36] In this study, we used VCAM-1 not as a marker for targeted plaque imaging, but as an inflammation marker in the context of endothelial regeneration after intravascular procedures. The detection of delayed reendothelialization and prolonged endothelial inflammation induced by diet or drug-eluting stents is an acute issue in clinical diagnostics. The results of our study open new perspectives to the application of molecular ultrasound for monitoring vascular healing in big vessels such as carotid arteries, which are the main arteries subjected to revascularization. Potential clinical translation was further encouraged by similar results collected in a pig model (own unpublished data).

Our study has limitations. First, using MB_{VCAM-1}, we can monitor endothelial regeneration and coverage, but this may not be equal to complete functional endothelial recovery. Thrombogenicity and complement activation may still be given even if VCAM-1 expression levels have been normalized. Therefore, other adhesion molecules involved in leukocyte recruitment and transendothelial migration, such as P-selectin,[37,38] should be investigated in future studies as well, to provide evidence for a functional endothelial recovery. Second, streptavidin-coated MBs are not clinically translatable, nor is the use of biotinylated antibodies. However, targeting peptides and antibodies can also be coupled using nonimmunogenic linkers. This was recently demonstrated with clinically applicable poly-*n*-butylcyanoacrylate MBs based on a peptide ligand for specific imaging of E-selectin expression in tumor blood vessels,[39] as well as with angiogenesis-specific $VEGFR_2$-MBs in molecular imaging of breast and prostate cancer,[40,41] and with P- and E-selectin–targeted MBs in inflammatory bowel disease[42] and myocardial infarction.[43] Following these examples of clinically translatable molecular ultrasound contrast agents, the generation of a MB_{VCAM-1} with covalently attached targeting ligands would be a logical and practicable next step for future clinical implementation. Moreover, metal stents are not suitable for ultrasound imaging because the acoustic reflectivity of the stent would obstruct MB detection and impede healing assessments. Consequently,

this diagnostic method can only be applied in case of polymer-based stents and after endarterectomy.

In conclusion, we demonstrate that noninvasive molecular ultrasound monitoring of vascular healing after intravascular procedures is possible through luminal exposure of VCAM-1 when using VCAM-1–targeted MBs as intravascular molecular probes. Therefore, molecular ultrasound imaging may become an important diagnostic tool supporting the development of adequate therapeutic strategies to reduce complications and to personalize anticoagulant and anti-inflammatory therapy after stent implantation or endarterectomy in carotid arteries for cerebral revascularization.

Acknowledgments

This Research was supported by the RWTH Aachen University IZKF core facility for Two-Photon Microscopy.

Sources of Funding

This Research was supported by the Deutsche Forschungsgemeinschaft Forschergruppe FOR809 and IZKF Aachen (Junior Research Group to Dr Liehn).

Disclosures

None.

References

1. Sternberg K, Grabow N, Petersen S, Weitschies W, Harder C, Ince H, Kroemer HK, Schmitz KP. Advances in coronary stent technology–active drug-loaded stent surfaces for prevention of restenosis and improvement of biocompatibility. *Curr Pharm Biotechnol*. 2013;14:76–90.
2. Lal BK. Recurrent carotid stenosis after CEA and CAS: diagnosis and management. *Semin Vasc Surg*. 2007;20:259–266. doi: 10.1053/j.semvascsurg.2007.10.009.
3. Napoli C, de Nigris F, Williams-Ignarro S, Pignalosa O, Sica V, Ignarro LJ. Nitric oxide and atherosclerosis: an update. *Nitric Oxide*. 2006;15:265–279. doi: 10.1016/j.niox.2006.03.011.
4. Otsuka F, Finn AV, Yazdani SK, Nakano M, Kolodgie FD, Virmani R. The importance of the endothelium in atherothrombosis and coronary stenting. *Nat Rev Cardiol*. 2012;9:439–453. doi: 10.1038/nrcardio.2012.64.
5. Chaabane C, Otsuka F, Virmani R, Bochaton-Piallat ML. Biological responses in stented arteries. *Cardiovasc Res*. 2013;99:353–363. doi: 10.1093/cvr/cvt115.
6. Seedial SM, Ghosh S, Saunders RS, Suwanabol PA, Shi X, Liu B, Kent KC. Local drug delivery to prevent restenosis. *J Vasc Surg*. 2013;57:1403–1414. doi: 10.1016/j.jvs.2012.12.069.
7. Siddiqi OK, Faxon DP. Very late stent thrombosis: current concepts. *Curr Opin Cardiol*. 2012;27:634–641. doi: 10.1097/HCO.0b013e3283587c7e.
8. Inoue T, Croce K, Morooka T, Sakuma M, Node K, Simon DI. Vascular inflammation and repair: implications for re-endothelialization, restenosis, and stent thrombosis. *JACC Cardiovasc Interv*. 2011;4:1057–1066. doi: 10.1016/j.jcin.2011.05.025.
9. Grote K, Sonnenschein K, Kapopara PR, Hillmer A, Grothusen C, Salguero G, Kotlarz D, Schuett H, Bavendiek U, Schieffer B. Toll-like receptor 2/6 agonist macrophage-activating lipopeptide-2 promotes reendothelialization and inhibits neointima formation after vascular injury. *Arterioscler Thromb Vasc Biol*. 2013;33:2097–2104. doi: 10.1161/ATVBAHA.113.301799.
10. Simsekyilmaz S, Cabrera-Fuentes HA, Meiler S, Kostin S, Baumer Y, Liehn EA, Weber C, Boisvert WA, Preissner KT, Zernecke A. Role of extracellular RNA in atherosclerotic plaque formation in mice. *Circulation*. 2014;129:598–606. doi: 10.1161/CIRCULATIONAHA.113.002562.
11. Lindner V, Collins T. Expression of NF-kappa B and I kappa B-alpha by aortic endothelium in an arterial injury model. *Am J Pathol*. 1996;148:427–438.
12. Fokong S, Theek B, Wu Z, Koczera P, Appold L, Jorge S, Resch-Genger U, van Zandvoort M, Storm G, Kiessling F, Lammers T. Image-guided, targeted and triggered drug delivery to tumors using polymer-based microbubbles. *J Control Release*. 2012;163:75–81. doi: 10.1016/j.jconrel.2012.05.007.
13. Koczera P, Wu Z, Fokong S, Theek B, Appold L, Jorge S, Möckel D, Liu Z, Curaj A, Storm G, van Zandvoort M, Kiessling F, Lammers T. Fluorescently labeled microbubbles for facilitating translational molecular ultrasound studies. *Drug Deliv Transl Res*. 2012;2:56–64. doi: 10.1007/s13346-011-0056-9.
14. Wu Z, Curaj A, Fokong S, Liehn EA, Weber C, Lammers T, Kiessling F, Zandvoort van M. Rhodamine-loaded intercellular adhesion molecule-1-targeted microbubbles for dual-modality imaging under controlled shear stresses. *Circ Cardiovasc Imaging*. 2013;6:974–981. doi: 10.1161/CIRCIMAGING.113.000805.
15. Rademakers T, Douma K, Hackeng TM, Post MJ, Sluimer JC, Daemen MJ, Biessen EA, Heeneman S, van Zandvoort MA. Plaque-associated vasa vasorum in aged apolipoprotein E-deficient mice exhibit proatherogenic functional features in vivo. *Arterioscler Thromb Vasc Biol*. 2013;33:249–256. doi: 10.1161/ATVBAHA.112.300087.
16. Curcio A, Torella D, Indolfi C. Mechanisms of smooth muscle cell proliferation and endothelial regeneration after vascular injury and stenting: approach to therapy. *Circ J*. 2011;75:1287–1296.
17. Tahir H, Bona-Casas C, Hoekstra AG. Modelling the effect of a functional endothelium on the development of in-stent restenosis. *PLoS One*. 2013;8:e66138. doi: 10.1371/journal.pone.0066138.
18. Ilan N, Madri JA. PECAM-1: old friend, new partners. *Curr Opin Cell Biol*. 2003;15:515–524.
19. Davies MJ, Gordon JL, Gearing AJ, Pigott R, Woolf N, Katz D, Kyriakopoulos A. The expression of the adhesion molecules ICAM-1, VCAM-1, PECAM, and E-selectin in human atherosclerosis. *J Pathol*. 1993;171:223–229. doi: 10.1002/path.1711710311.
20. Zeiffer U, Schober A, Lietz M, Liehn EA, Erl W, Emans N, Yan ZQ, Weber C. Neointimal smooth muscle cells display a proinflammatory phenotype resulting in increased leukocyte recruitment mediated by P-selectin and chemokines. *Circ Res*. 2004;94:776–784. doi: 10.1161/01.RES.0000121105.72718.5C.
21. Schober A, Zernecke A, Liehn EA, von Hundelshausen P, Knarren S, Kuziel WA, Weber C. Crucial role of the CCL2/CCR2 axis in neointimal hyperplasia after arterial injury in hyperlipidemic mice involves early monocyte recruitment and CCL2 presentation on platelets. *Circ Res*. 2004;95:1125–1133. doi: 10.1161/01.RES.0000149518.86865.3e.
22. Kennedy S, McPhaden AR, Wadsworth RM, Wainwright CL. Correlation of leukocyte adhesiveness, adhesion molecule expression and leukocyte-induced contraction following balloon angioplasty. *Br J Pharmacol*. 2000;130:95–103. doi: 10.1038/sj.bjp.0703282.
23. Cybulsky MI, Iiyama K, Li H, Zhu S, Chen M, Iiyama M, Davis V, Gutierrez-Ramos JC, Connelly PW, Milstone DS. A major role for VCAM-1, but not ICAM-1, in early atherosclerosis. *J Clin Invest*. 2001;107:1255–1262. doi: 10.1172/JCI11871.
24. Kaufmann BA, Carr CL, Belcik JT, Xie A, Yue Q, Chadderdon S, Caplan ES, Khangura J, Bullens S, Bunting S, Lindner JR. Molecular imaging of the initial inflammatory response in atherosclerosis: implications for early detection of disease. *Arterioscler Thromb Vasc Biol*. 2010;30:54–59. doi: 10.1161/ATVBAHA.109.196386.
25. Khanicheh E, Mitterhuber M, Xu L, Haeuselmann SP, Kuster GM, Kaufmann BA. Noninvasive ultrasound molecular imaging of the effect of statins on endothelial inflammatory phenotype in early atherosclerosis. *PLoS One*. 2013;8:e58761. doi: 10.1371/journal.pone.0058761.
26. Khanicheh E, Qi Y, Xie A, Mitterhuber M, Xu L, Mochizuki M, Daali Y, Jaquet V, Krause KH, Ruggeri ZM, Kuster GM, Lindner JR, Kaufmann BA. Molecular imaging reveals rapid reduction of endothelial activation in early atherosclerosis with apocynin independent of antioxidative properties. *Arterioscler Thromb Vasc Biol*. 2013;33:2187–2192. doi: 10.1161/ATVBAHA.113.301710.
27. Qu Y, Shi X, Zhang H, Sun W, Han S, Yu C, Li J. VCAM-1 siRNA reduces neointimal formation after surgical mechanical injury of the rat carotid artery. *J Vasc Surg*. 2009;50:1452–1458. doi: 10.1016/j.jvs.2009.08.050.
28. Nakashima Y, Raines EW, Plump AS, Breslow JL, Ross R. Upregulation of VCAM-1 and ICAM-1 at atherosclerosis-prone sites on the endothelium in the ApoE-deficient mouse. *Arterioscler Thromb Vasc Biol*. 1998;18:842–851.
29. Bobryshev YV, Lord RS, Rainer SP, Munro VF. VCAM-1 expression and network of VCAM-1 positive vascular dendritic cells in advanced atherosclerotic lesions of carotid arteries and aortas. *Acta Histochem*. 1996;98:185–194. doi: 10.1016/S0065-1281(96)80037-7.
30. Hastings NE, Feaver RE, Lee MY, Wamhoff BR, Blackman BR. Human IL-8 regulates smooth muscle cell VCAM-1 expression in response to

endothelial cells exposed to atheroprone flow. *Arterioscler Thromb Vasc Biol*. 2009;29:725–731. doi: 10.1161/ATVBAHA.109.184382.
31. Seitz O, Schürmann C, Hermes N, Müller E, Pfeilschifter J, Frank S, Goren I. Wound healing in mice with high-fat diet- or ob gene-induced diabetes-obesity syndromes: a comparative study. *Exp Diabetes Res*. 2010;2010:476969. doi: 10.1155/2010/476969.
32. Nascimento AP, Costa AM. Overweight induced by high-fat diet delays rat cutaneous wound healing. *Br J Nutr*. 2006;96:1069–1077.
33. Marin C, Ramirez R, Delgado-Lista J, Yubero-Serrano EM, Perez-Martinez P, Carracedo J, Garcia-Rios A, Rodriguez F, Gutierrez-Mariscal FM, Gomez P, Perez-Jimenez F, Lopez-Miranda J. Mediterranean diet reduces endothelial damage and improves the regenerative capacity of endothelium. *Am J Clin Nutr*. 2011;93:267–274. doi: 10.3945/ajcn.110.006866.
34. Roelke LH, Rodrigues SL, Lotufo PA, Mill JG. Correlation between the intima-media thickness of the proximal and distal common carotids. *Arq Bras Cardiol*. 2013;101:211–216. doi: 10.5935/abc.20130151.
35. Clevert DA, Sommer WH, Helck A, Reiser M. Duplex and contrast enhanced ultrasound (CEUS) in evaluation of in-stent restenosis after carotid stenting. *Clin Hemorheol Microcirc*. 2011;48:199–208. doi: 10.3233/CH-2011-1400.
36. Bauer M, Caviezel S, Teynor A, Erbel R, Mahabadi AA, Schmidt-Trucksäss A. Carotid intima-media thickness as a biomarker of subclinical atherosclerosis. *Swiss Med Wkly*. 2012;142:w13705. doi: 10.4414/smw.2012.13705.
37. Bettinger T, Bussat P, Tardy I, Pochon S, Hyvelin JM, Emmel P, Henrioud S, Biolluz N, Willmann JK, Schneider M, Tranquart F. Ultrasound molecular imaging contrast agent binding to both E- and P-selectin in different species. *Invest Radiol*. 2012;47:516–523. doi: 10.1097/RLI.0b013e31825cc605.
38. Deshpande N, Lutz AM, Ren Y, Foygel K, Tian L, Schneider M, Pai R, Pasricha PJ, Willmann JK. Quantification and monitoring of inflammation in murine inflammatory bowel disease with targeted contrast-enhanced US. *Radiology*. 2012;262:172–180. doi: 10.1148/radiol.11110323.
39. Fokong S, Fragoso A, Rix A, Curaj A, Wu Z, Lederle W, Iranzo O, Gätjens J, Kiessling F, Palmowski M. Ultrasound molecular imaging of E-selectin in tumor vessels using poly n-butyl cyanoacrylate microbubbles covalently coupled to a short targeting peptide. *Invest Radiol*. 2013;48:843–850. doi: 10.1097/RLI.0b013e31829d03ec.
40. Bachawal SV, Jensen KC, Lutz AM, Gambhir SS, Tranquart F, Tian L, Willmann JK. Earlier detection of breast cancer with ultrasound molecular imaging in a transgenic mouse model. *Cancer Res*. 2013;73:1689–1698. doi: 10.1158/0008-5472.CAN-12-3391.
41. Tardy I, Pochon S, Theraulaz M, Emmel P, Passantino L, Tranquart F, Schneider M. Ultrasound molecular imaging of VEGFR2 in a rat prostate tumor model using BR55. *Invest Radiol*. 2010;45:573–578. doi: 10.1097/RLI.0b013e3181ee8b83.
42. Wang H, Machtaler S, Bettinger T, Lutz AM, Luong R, Bussat P, Gambhir SS, Tranquart F, Tian L, Willmann JK. Molecular imaging of inflammation in inflammatory bowel disease with a clinically translatable dual-selectin-targeted US contrast agent: comparison with FDG PET/CT in a mouse model. *Radiology*. 2013;267:818–829. doi: 10.1148/radiol.13122509.
43. Davidson BP, Kaufmann BA, Belcik JT, Xie A, Qi Y, Lindner JR. Detection of antecedent myocardial ischemia with multiselectin molecular imaging. *J Am Coll Cardiol*. 2012;60:1690–1697. doi: 10.1016/j.jacc.2012.07.027.

Significance

Thrombotic arterial occlusion because of endothelial damage is the main limitation of interventional blood flow restoration in atherosclerotic arteries. The current recommendation is a preventive anticoagulant therapy for at least 12 months in case of drug-eluting stent implantation. However, anticoagulant therapy limits further surgical interventions and can also cause adverse effects, such as cerebral hemorrhage. Thus, it should be administered as short as necessary. Unfortunately, the optimal duration of antiplatelet therapy after various revascularization procedures remains unknown because of uncertainty of endothelial recovery. Molecular ultrasound imaging is an exquisite tool for characterizing angiogenic and inflammatory vessels and initial clinical trials with targeted microbubbles show promising results. In this article, we provide preclinical evidence that VCAM-1–targeted microbubbles faithfully depict vessel damage and endothelial regeneration. On the basis of these findings, we hypothesize that molecular ultrasound imaging may become a powerful diagnostic tool to personalize antiplatelet therapy after vascular interventions, capable of improving the therapeutic outcome of patients.

Arteriosclerosis, Thrombosis, and Vascular Biology

JOURNAL OF THE AMERICAN HEART ASSOCIATION

Noninvasive Molecular Ultrasound Monitoring of Vessel Healing After Intravascular Surgical Procedures in a Preclinical Setup

Adelina Curaj, Zhuojun Wu, Stanley Fokong, Elisa A. Liehn, Christian Weber, Alexandrina Burlacu, Twan Lammers, Marc van Zandvoort and Fabian Kiessling

Arterioscler Thromb Vasc Biol. 2015;35:1366-1373; originally published online April 2, 2015;
doi: 10.1161/ATVBAHA.114.304857
Arteriosclerosis, Thrombosis, and Vascular Biology is published by the American Heart Association, 7272 Greenville Avenue, Dallas, TX 75231

Print ISSN: 1079-5642. Online ISSN: 1524-4636

Data supplement

Synthesis of poly n-butylcyanoacrylate target-specific MBs

Rhodamine loaded poly-n-butylcyanoacrylate (PBCA)–stabilized, air-filled MBs were prepared and functionalized as previously described [1, 2]. $1x10^7$ streptavidin-coated MBs in HEPES/Triton buffer (pH 7.0) were mixed with 5 µg of biotinylated anti-VCAM-1 antibody (clone 429, eBioscience) and incubated at room temperature for 30 min. Conjugated MBs were separated from excess antibody by 30 min flotation and re-suspended in 50 µL HEPES/Triton buffer.

Atherogenic murine model of restenosis

Animal experiments were approved by local authorities and complied with the European Convention of Animal Protection law. Two similar animal models of accelerated atherosclerosis were used in this study: 1) eight-week old $ApoE^{-/-}$ mice were fed an atherogenic diet (Altromin, Germany) for 1 week before and 2 weeks after the carotid injury (named short-term diet group); 2) mice were fed an atherogenic diet for 12 weeks before and 2 weeks after the arterial denudation (named long-term diet group). The arterial injury was performed using a coated guide wire as previously described [3]. A total number of 122 animals were used for this study, consisting of n=29 for *ex vivo* TPLSM studies, n=15 for immunohistology, n=12 for *ex vivo* US, n=25 for *in vivo* TPLSM and n=41 for *in vivo* US. Following the wire-injury procedure, VCAM-1 expression was measured at different time points (1, 3, 7, 14 days post-injury).

Operative procedures for flow-chamber experiments

For each time point (1, 3, 7, 14 d) after arterial injury, mice were killed by intraperitoneal (i.p.) overdose injection of 400 mg/ml ketamine and 40 mg/ml xylazine. In addition, a terminal blood collection was performed via intracardiac puncture. The common carotid arteries (6-7 mm) were excised by restricted handling of both ends of the blood vessel to exclude luminal alterations. In order to avoid air bubbles within the lumen and tissue dryness, the blood vessels were preserved at 4°C in 1x Hanks Balanced Salt Solution (HBSS, pH 7.4, Life Technologies) during *ex vivo* imaging preparations. Each excised carotid artery was mounted in a customized flow chamber and then filled with HBSS (37°C) as previously described [4]. For the US flow chamber experiments, we used a 7 cm deep flow-chamber to ensure US-waves propagation and the carotid artery was brought into the field of view by immersing the scan-head into the liquid. To mimic physiological conditions inside the mounted carotid arteries, fresh blood collected from healthy volunteers was anti-coagulated with heparin (10 U/ml) - EDTA (1.2 - 2 mg EDTA/ml) and infused through the carotids preserving the physiological flow direction. Subsequently, MBs suspended in whole blood, were infused for 10 min, followed by a 4 min washing step using human blood and a second washing step using HBSS.

Ex vivo whole mount artery TPLSM imaging of wire-injured carotids

Animals (n=20) were operated as described above. At 1, 3, 7 and 14 d post-surgery, mice (n=5, for each time point) were sacrificed via overdose i.p. injection of anesthetics. After mounting and flushing the carotids, cell nuclei (SYTO 41), endothelial PECAM-1 (CD31), and VCAM-1 (CD106) were stained by an one-step incubation. 400 µl of HBSS containing anti-CD31 Oregon Green 488 (2.5 µg/mL), anti-CD106 Alexa Fluor 568 (2.5 µg/mL), and SYTO 41 (5 nM) were used to flush the carotid artery. Incubation was performed at transluminal pressure of 80 mmHg for 1 h. After flushing the artery with HBSS, imaging was performed using an Olympus FV1000MPE multiphoton microscopy system (Mai Tai DeepSee pulsed Ti:Sapphire laser with 140 fs pulse width at an excitation wavelength of 800 nm). A 25x water dipping objective with numeric aperture (NA) of 1.05, working distance (WD) of 2 mm, and with optical zoom capability was used. Three internal photon multiplier tubes were used to detect the fluorescence signals and filters were adjusted to the corresponding spectra: 418- 468 nm for SYTO 41, 495-540 nm for elastin autofluorescence and CD31, and 595-650 nm for CD106. TPLSM images were analyzed using Image-Pro Analyzer 7.0 software (Media Cybernetis, Inc.) and Imaris software (Bitplane).

Flow chamber experiments on the binding of MB_{VCAM-1} to carotid arteries after wire-injury using molecular US

High-resolution imaging of the excised carotid arteries 1 d after the arterial denudation (n=12) was performed with a linear high-frequency transducer (55 MHz, mechanical index 0.9, peak negative pressure 6.7 MPa, axial resolution 30 µm, lateral resolution 70 µm, focal length 4.5 mm, depth of field 1.4 mm, field of view 10.9 mm) connected to a small animal US imaging system (Vevo 770, VisualSonics Inc) using a long-axis imaging plane. Measurements were performed using the contrast mode, which makes use of the enhanced scattering of MBs at low US energies (4% power, mechanical index 0.04) to distinguish them from tissue response. Ten minutes after MBs infusion, a visible steady-state confirmed a homogeneous MBs distribution in the circulating blood before the destructive pulse (Figure 3). After 10 min of continuous flow, the MBs-blood mixture was removed from the circuit by two washing steps (first with blood and then with HBSS as mentioned above). For competitive binding experiments, the carotid lumen was incubated with a 20-fold higher concentration of free anti-CD106 antibody (100 µg, 2 µg/µl) for 1 h prior to MBs injection. To quantify the amount of bound MBs in the imaged area, an imaging sequence of 60 seconds (10 frames/second) was acquired. To prevent MBs destruction, the first third of the sequence recorded images at a low transducer output power of 4%. Subsequently, a destructive pulse (100% power) destroyed all MBs in the imaged area. The remaining imaging sequence was acquired at 4% power. Image analysis was performed by subtracting the mean value of grayscale intensity for several post-destructive frames (HBSS only) from the mean value of several pre-destructive frames (bound MBs). The resulting grayscale intensity difference represents the amount of signal generated by stationary MBs.

Flow chamber experiments on the binding of MB_{VCAM-1} to carotid arteries after wire-injury using TPLSM

Three days post wire-injury, animals (n=9) were sacrificed and the carotid arteries were mounted as described above. Prior to the binding step, the arteries were stained with OG488 labelled endothelial PECAM-1 (CD31) and SYTO 41. For competitive binding experiments, the carotid lumen was incubated with a 20x higher free anti-CD106 antibody concentration for 1 h prior to MB injection. After the infusion of MBs and washing, imaging was performed using the Olympus FV1000MPE multiphoton microscopy systems. PECAM, SYTO 41 and CD106 filter settings were selected as described above. Rhodamine-labeled MBs were imaged using an excitation wavelength of 840 nm and a spectral filter for the ranging 595-650 nm.

In vivo molecular US imaging

Mice with wire-injured carotid arteries (n=41) were investigated by molecular US imaging at different time points (1, 3, 7 and 14 d). For catheterization and imaging the mice were anaesthetized with 1% isoflurane and placed on a heated table (Vevo Mouse Handling Table). *In vivo* molecular US measurements were performed using a small animal high frequency US system (Vevo 770, VisualSonics) and a 40 MHz transducer (mechanical index 1.2, peak negative pressure 6.6 MPa, axial resolution 40 µm, lateral resolution 80 µm, focal length 6 mm, depth of field 1.5 mm, field of view 14.5 mm). MB-specific signals were acquired and color-coded overlays on B-mode images were performed using the contrast mode provided by the vendor. A dose of $2x10^7$ MB_{VCAM-1} or MBs control (MB_{CTR}) was injected intravenously via the cannulated tail vein under US control (4% transmitted power, mechanical index 0.036). For competitive binding studies at 1 d after wire-injury, intravenous injection of 20-fold higher concentration of free anti-CD106 antibody (100 µg, 2 µg/µl) was applied to each mouse 10 min before MB_{VCAM-1} injection to block VCAM-1-binding sites. In all experiments successful MB injection was confirmed by assessing an imaging sequence of 60 seconds (10 frames/second) during the injection. Seven minutes after MB injection, molecular US imaging in contrast mode was performed as described above to measure the difference in the signal levels before and directly after the destructive pulse [5].

In vivo TPLSM

For *in vivo* measurements, wire-injured ApoE $^{-/-}$ mice (n=25) were anesthetized using an i.p. injection of ketamine (100 mg/kg) and medetomidine (10 mg/kg). Body temperature was kept at 37°C by means of a heating pad. Then, the carotid artery was carefully exposed. For MB injections, a catheter made of a 0.28 mm polyethylene tubing adapted to a 30 G needle was inserted into the tail vein and flushed with NaCl-heparin solution. Thirty minutes before imaging 0.5 nM SYTO 13 was applied superficially on the top of the exposed carotid in order to stain the vessel adventitia for orientation within the tissue.
TPLSM imaging was performed using a Leica SP5 (Leica Microsystems, Germany) with an integrated resonance scanner for high-speed imaging and a Compact

Ultrafast Ti:Sapphire Laser (Chameleon, Coherent, USA) at an excitation wavelength of 800 nm and a 20x water dipping objective (NA=1.0, WD=2 mm, with optical zoom capability). Two internal photon multiplier tubes were used to detect the fluorescence signals and filters were adjusted to the corresponding spectra: 505- 560 nm for SYTO 13, 590-650 nm for rhodamine. *In vivo* imaging was performed at a frame size of 400 x 400 pixels and with a scan rate of 8000 Hz. Line averaging of 2 was applied for noise reduction, resulting in a final imaging speed of 10 frames per second. For time lapse recording, a series of 500 images or 55 second of video material was recorded. After the injection of $8x10^7$ MB_{VCAM-1}, the carotid was imaged for 15 min. The animals were sacrificed after *in vivo* imaging and additional *ex vivo* carotid imaging at higher resolution was performed, as described above.

Immunohistology of denudated arteries from long-term diet group

Mice (n=15) fed for 12 weeks with an atherogenic diet (HFD) were subjected to arterial denudation and then sacrificed at different time point (1, 3, 7, 14 and 21 d). For immunhistology, perfusion fixation with 4% paraformaldehyde (P-6148, Sigma) and paraffin embedding was performed. Serial tissue sections (5 µm) were generated starting at the bifurcation. Samples were stained for VCAM-1 (11444-1-AP) and CD31 (sc-1506) expression. FITC-, respectively Cy5 conjugated secondary antibodies were used for visualization, and sections were analyzed using the „Diskus" software (Hilgers).

Statistical analysis

Differences between groups of *ex vivo* and *in vivo* MB adhesion assays were analyzed using the two-tailed Student's t-test, considering $p<0.05$ to display significant differences. To correct for multiple group comparisons, we performed Bonferroni correction. Error bars shown on graphs represent the standard deviation. Statistical analysis was performed using GraphPad Prism 5.0 (GraphPad Software).

Supplemental References:

1. Fokong S, Siepmann M, Liu Z, Schmitz G, Kiessling F, Gatjens J. Advanced characterization and refinement of poly N-butyl cyanoacrylate microbubbles for ultrasound imaging. *Ultrasound Med Biol.* 2011;37:1622-1634.

2. Fokong S, Theek B, Wu Z, Koczera P, Appold L, Jorge S, Resch-Genger U, van Zandvoort M, Storm G, Kiessling F, Lammers T. Image-guided, targeted and triggered drug delivery to tumors using polymer-based microbubbles. *J Control Release.* 2012;163:75-81.

3. Schober A, Zernecke A, Liehn EA, von Hundelshausen P, Knarren S, Kuziel WA, Weber C. Crucial role of the CCL2/CCR2 axis in neointimal hyperplasia after arterial injury in hyperlipidemic mice involves early monocyte recruitment and CCL2 presentation on platelets. *Circ Res.* 2004;95:1125-1133.

4. Wu Z, Curaj A, Fokong S, Liehn EA, Weber C, Lammers T, Kiessling F, Zandvoort van M. Rhodamine-Loaded Intercellular Adhesion Molecule-1-targeted Microbubbles for Dual-Modality Imaging Under Controlled Shear Stresses. *Circ Cardiovasc Imaging.* 2013;6:974-981.
5. Kiessling F, Bzyl J, Fokong S, Siepmann M, Schmitz G, Palmowski M. Targeted ultrasound imaging of cancer: an emerging technology on its way to clinics. *Curr Pharm Des.* 2012;18:2184-2199.

SUPPLEMENTAL MATERIAL

Supplemental Table

Supplemental Table I: Summary of the findings in literature about arterial endothelial and subendothelial marker expression.

Markers	Subendothelial expression	Activated endothelial expression	Constitutional endothelial expression
PECAM-1	- (1)	+ (1,2)	+ (1,2)
ICAM-1	+ (3) *	+ (2,4)	+ (2,4)
VCAM-1	+ (3)	+ (2,5,6)	- (2,6)
E-Selectin	- (7)	+ (2)	+ (2)
P-Selectin	- (7,8)	+ (7) **	+ (9)

* own expertise: almost no subendothelial expression of ICAM-1 was found (see Figure S2)

** own expertise: specific P-selectin signals could not conclusively be detected on remaining endothelial cells but only on attached platelets (see Supplemental Figure 5)

Supplemental Figures and Figure Legends

Supplemental Figure I

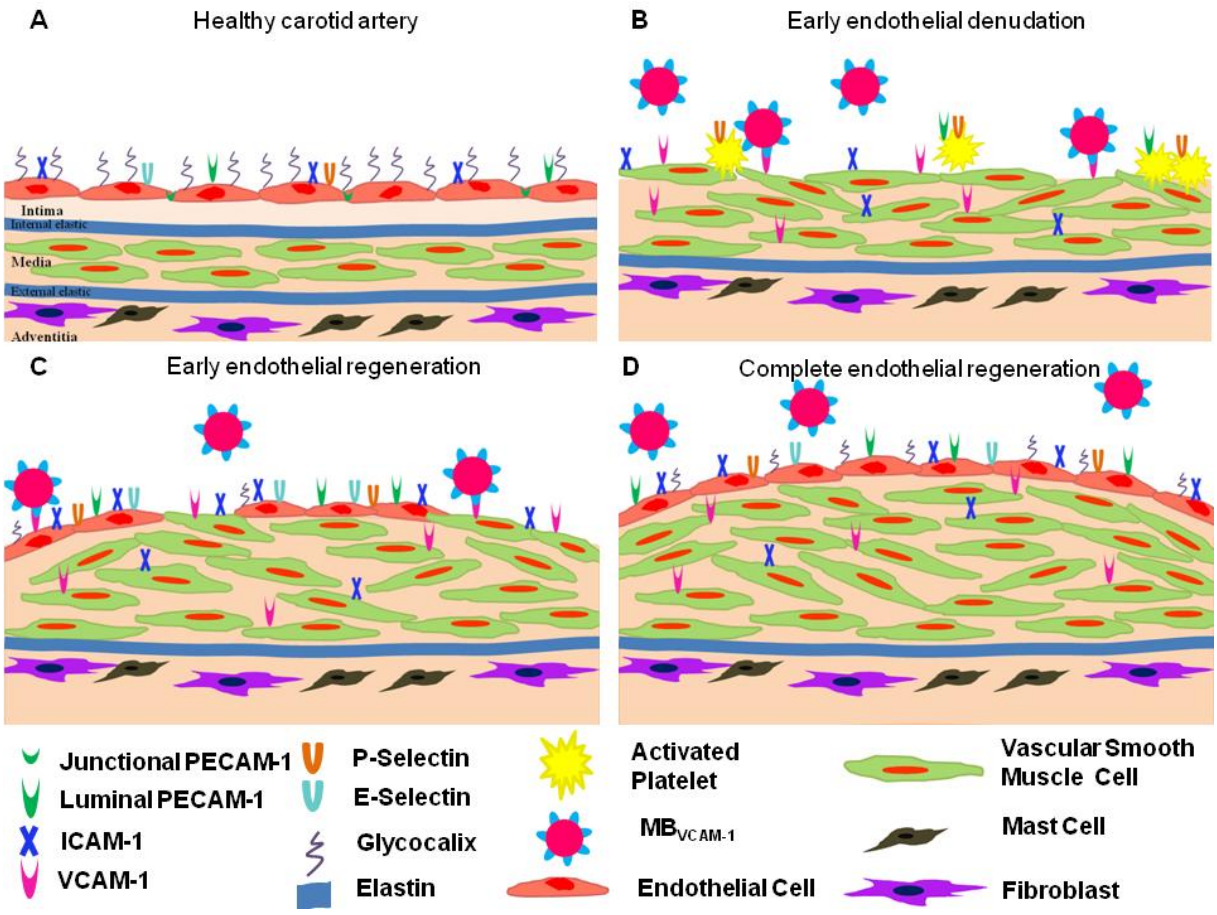

Supplemental Figure I: Scheme depicting the expression of luminal markers in healthy and wire-injured carotid arteries and its impact on MB_{VCAM-1}-binding. A) endothelium constitutively expresses PECAM-1, ICAM-1, P- and E-Selectin. B) after endothelial denudation, VSMC-related VCAM-1 and ICAM-1, as well as PECAM-1 and P-Selectin on attached thrombocytes are available on the luminal side of the artery. C) during endothelial recovery, PECAM-1, ICAM-1, VCAM-1, P- and E-Selectin are upregulated on ECs. VSMCs continue to express VCAM-1 and ICAM-1. D) even after the endothelium is completely reconstructed, PECAM-1, ICAM-1, P- and E-Selectin will still be available on the luminal site for a prolonged period of time, while VSMC-related VCAM-1 and ICAM-1 become inaccessible for intravascular molecular targeting.

Supplemental Figure II

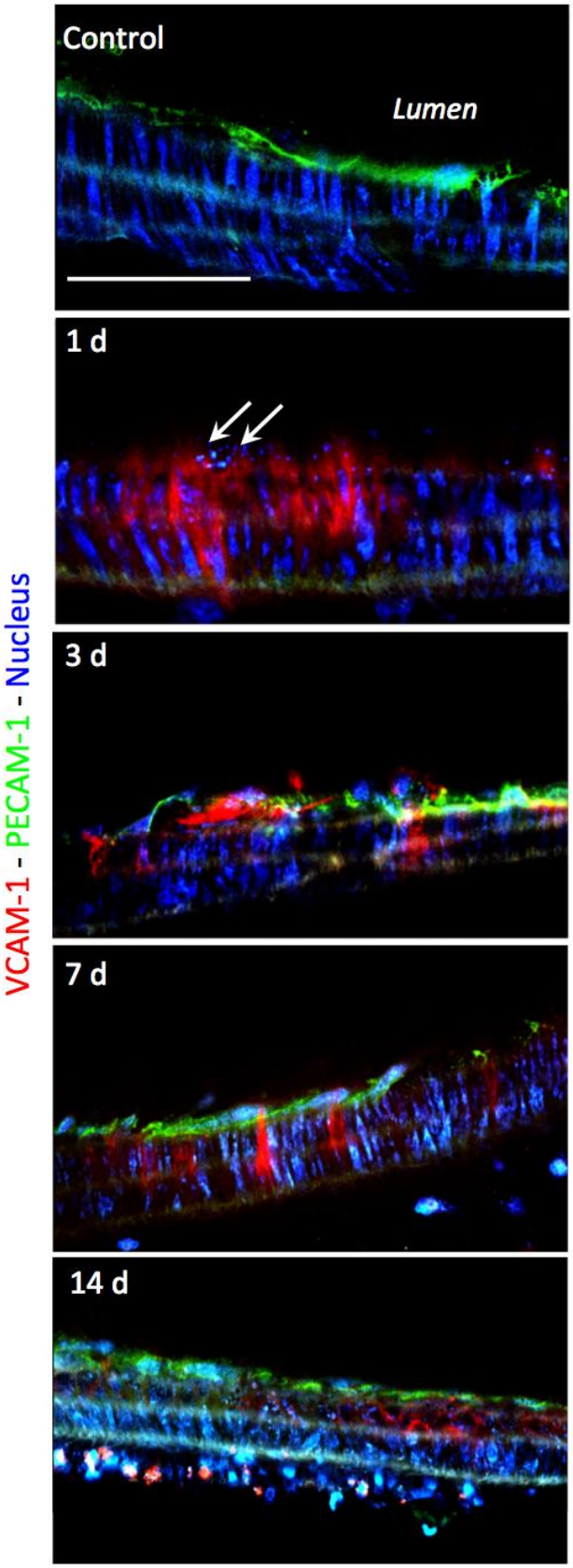

Supplemental Figure II: *Ex vivo* whole mount staining and TPLSM imaging of denudated carotid arteries of mice from short-term atherogenic diet group. For the staging of endothelial regeneration and VCAM-1 expression, mice were sacrificed at timepoint 1,3,7 and 14 d post denudation and the vital tissue was mounted and stained. One day post surgery, the endothelium (green = PECAM-1) is absent, showing only ECs debris in the lumen (indicated by white arrows). The VCAM-1-expressing VSMCs are exposed to the blood flow (red = VCAM-1). Three days post denudation, at the onset of endothelial regeneration, there is strong expression of VCAM-1 by both VSMCs and ECs (blue = SYTO 41). Seven days post denudation, there is a partial reconstruction of the endothelial layer covering VCAM-1-positive VSMCs. A complete endothelial recovery is found after 14 d. Images were processed using Image Pro 7.0. Scale bar=50 µm.

Supplemental Figure III

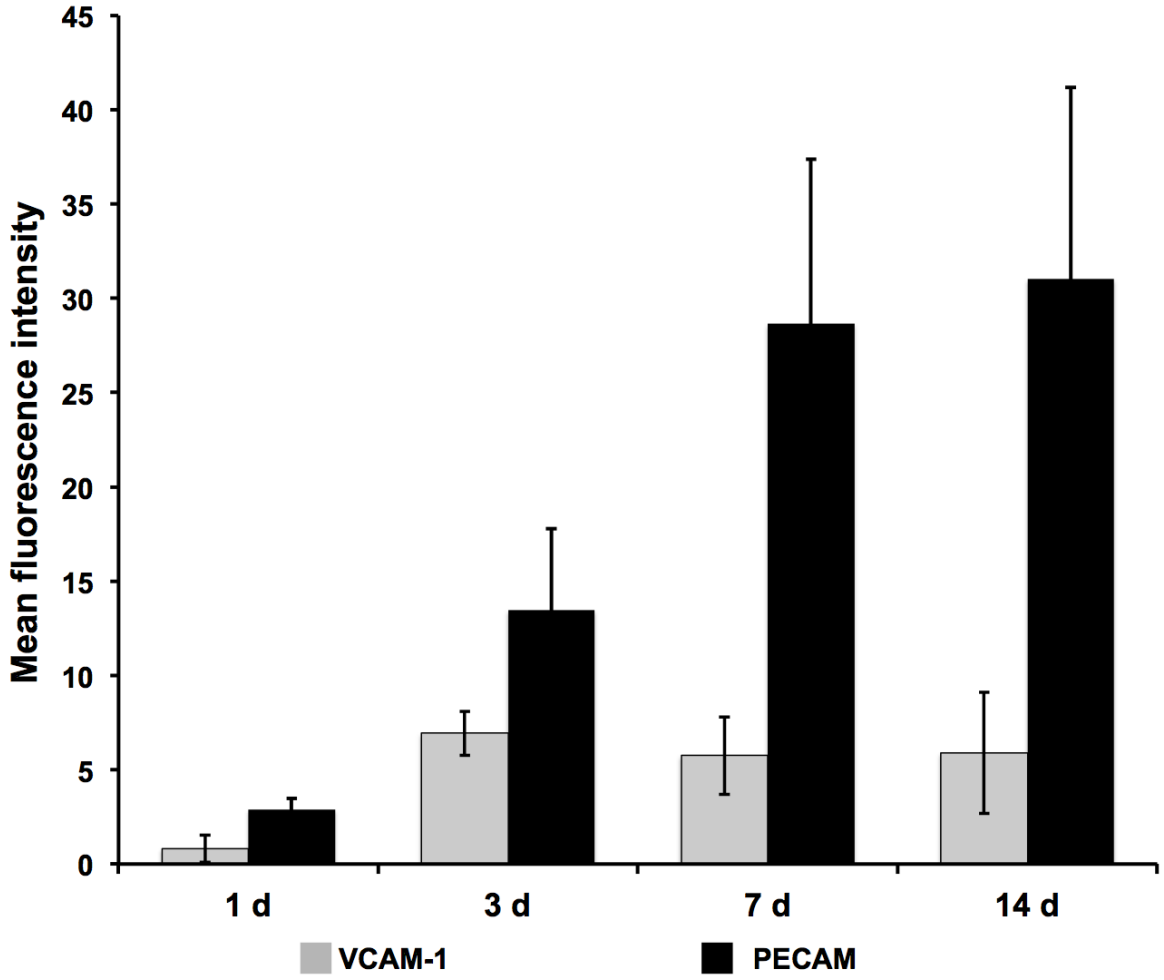

Supplemental Figure III: Mean fluorescence intensity measurement of VCAM-1 and PECAM expression after endothelial denudation in carotid arteries.

Supplemental Figure IV

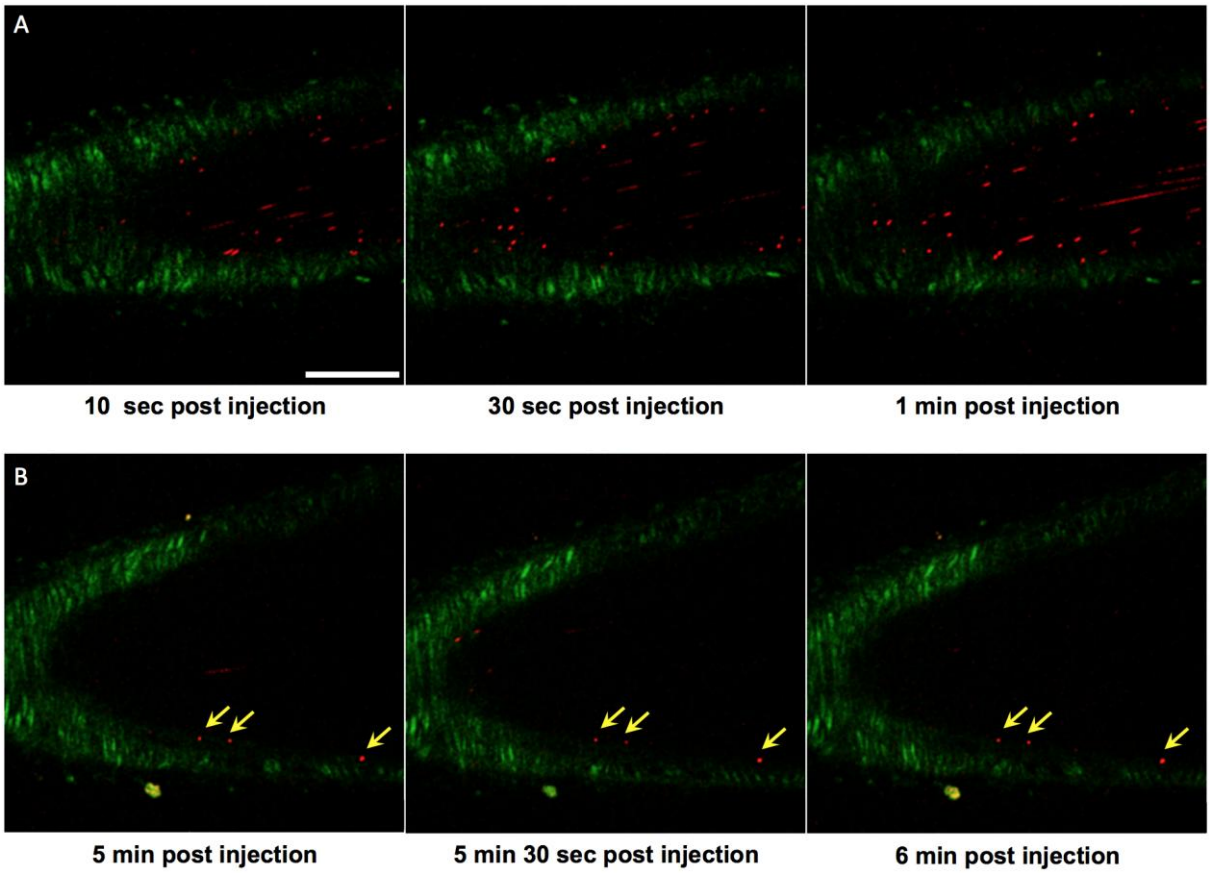

Supplemental Figure IV: *In vivo* TPLSM images of wire-injured carotid arteries at 3 d post surgery. A) Directly after the injection of $8x10^7$ MB_{VCAM-1}, the MBs circulate in the vessel lumen. B) Five minutes after MB_{VCAM-1} injection, circulating MB_{VCAM-1} are cleared out and only MB_{VCAM-1} (yellow arrows) bound to the injured vascular wall remain. For orientation, cells in adventitia and media are stained with SYTO 41 (green). MB_{VCAM-1} are labeled with rhodamine (red). Scale bar = 100 µm.

Supplemental Figure V

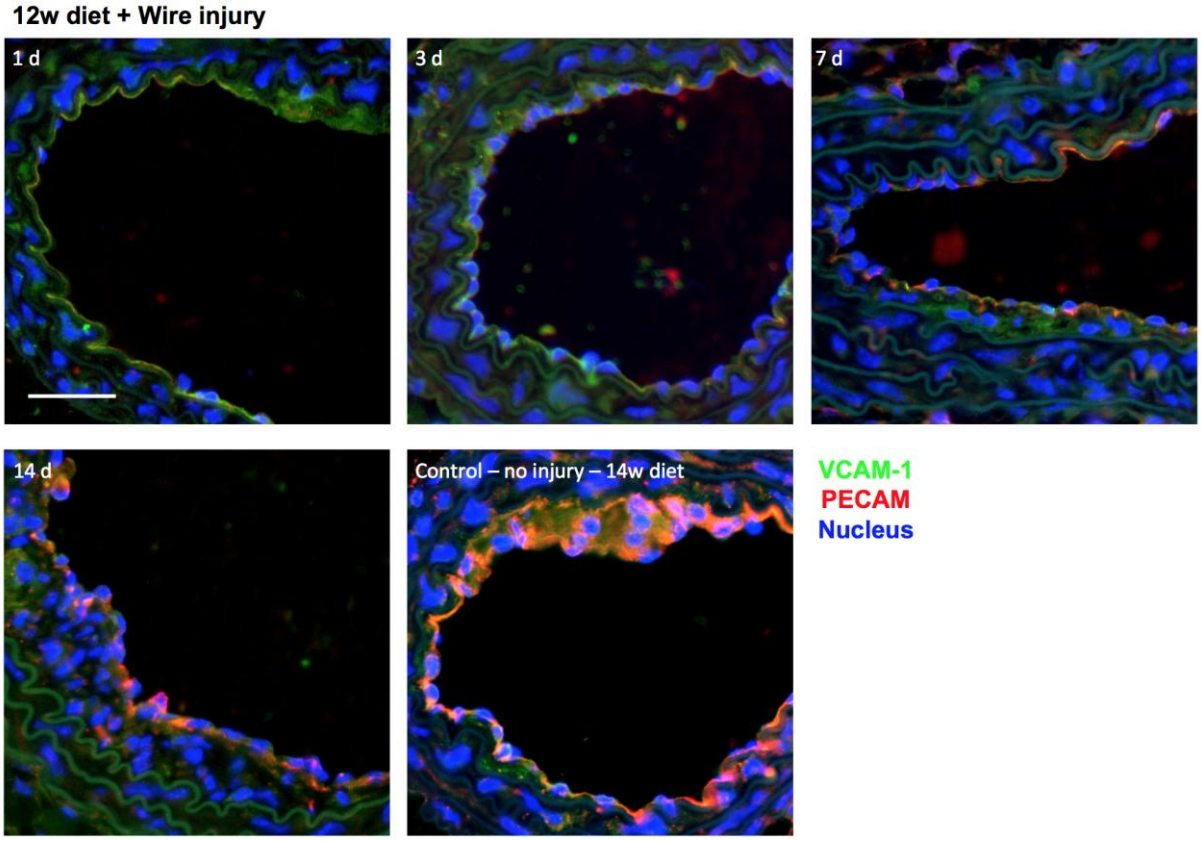

Supplemental Figure V: Immunofluorescence staining of wire-injured carotids after 12 weeks of high cholesterol diet. Scale bar = 50 μm.

Supplemental Figure VI

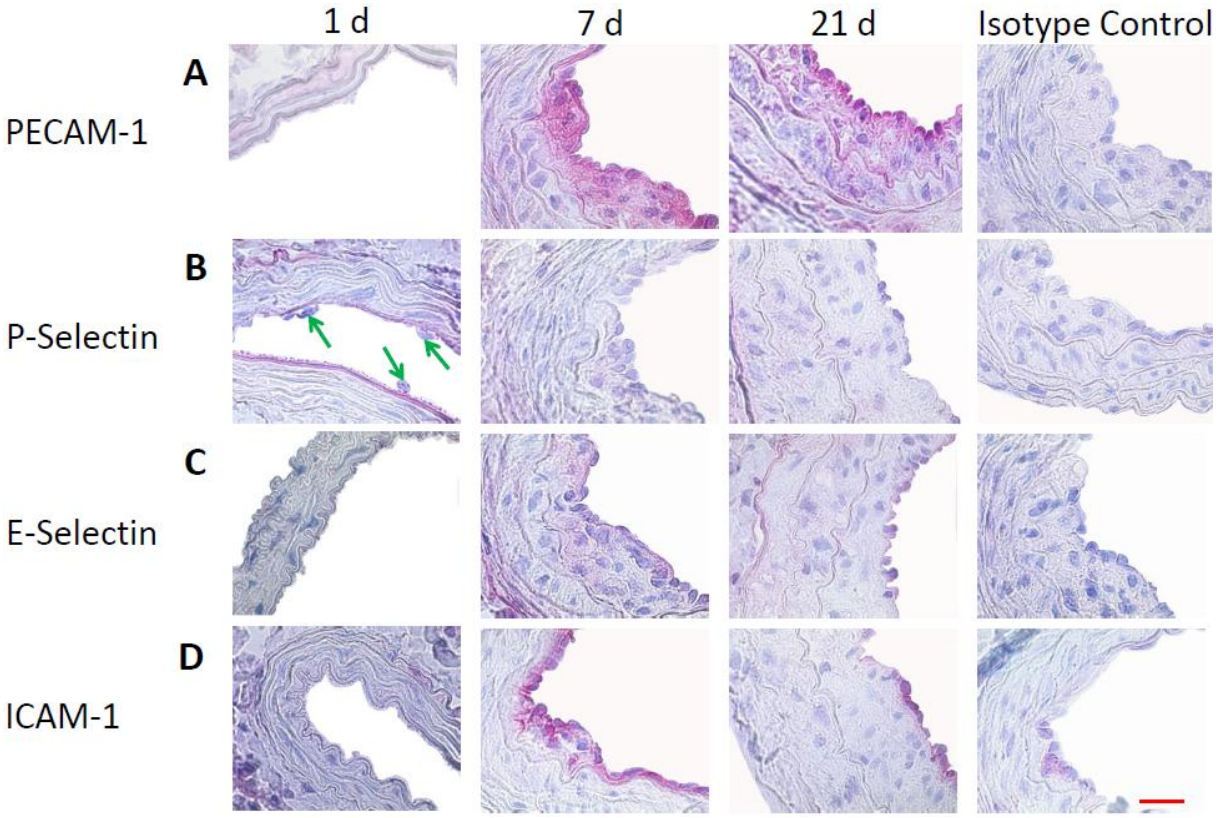

Supplemental Figure VI: Immunohistochemistry of wire-injured carotid arteries. One day after arterial injury, PECAM-1, E-Selectin and ICAM-1 staining showed no expression of these markers on the luminal side of the artery (A, C and D). P-Selectin could be detected on thrombocytes covering the denudated artery at 1 d, but hardly on the remaining ECs (green arrows). At 7 and 21 d, the endothelial layer expresses high levels of PECAM-1 and ICAM-1 (A and D), moderate levels of E-Selectin (C), but hardly any P-Selectin (B). Scale bar = 20 µm.

Supplemental Figure VII

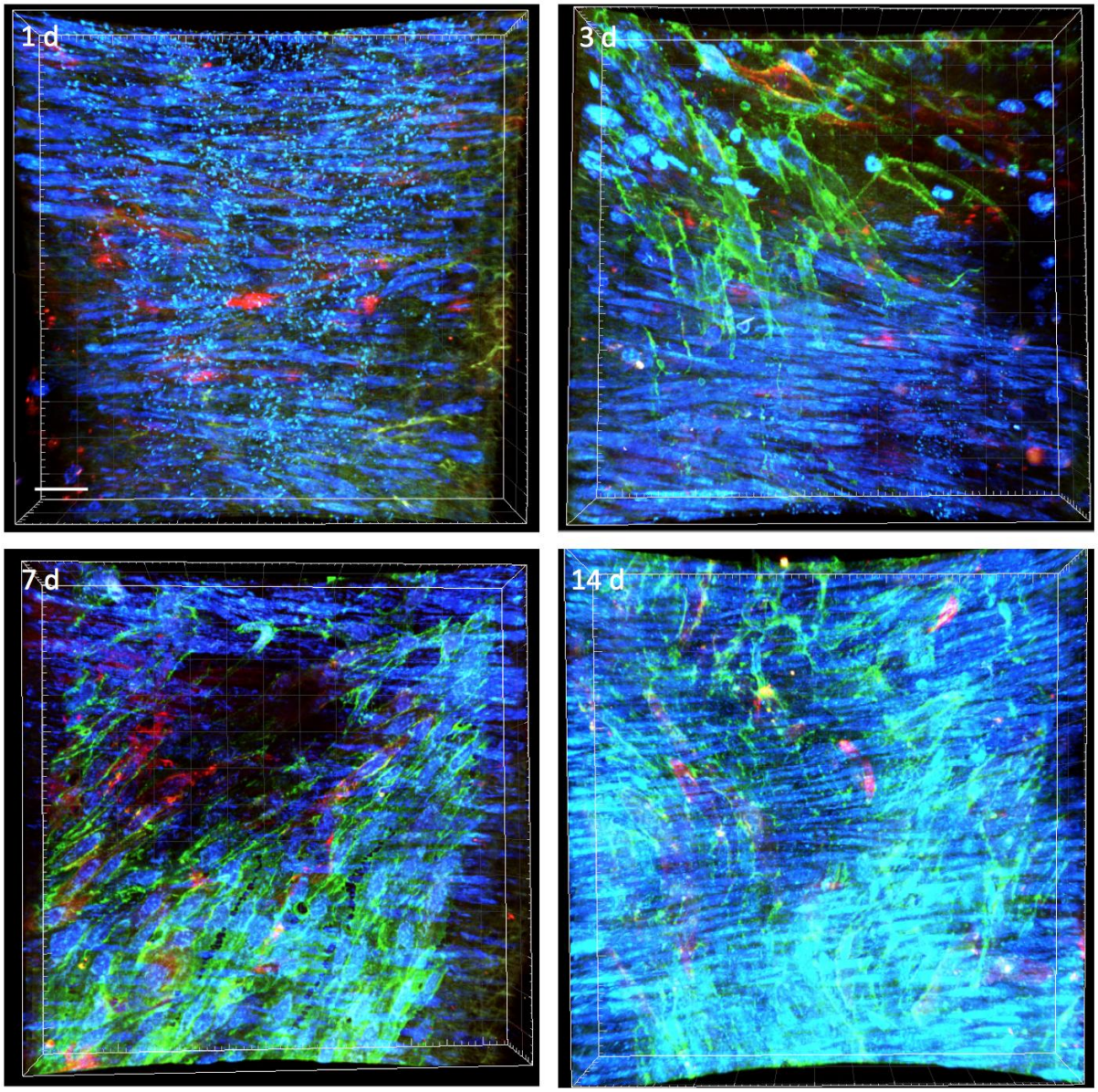

Supplemental Figure VII: Raw images of VCAM-1 and PECAM ex vivo staining before 3D-rendering (green = PECAM, red = VCAM-1, blue = nucleus, scale bar = 50 µm)

Supplemental Figure VIII

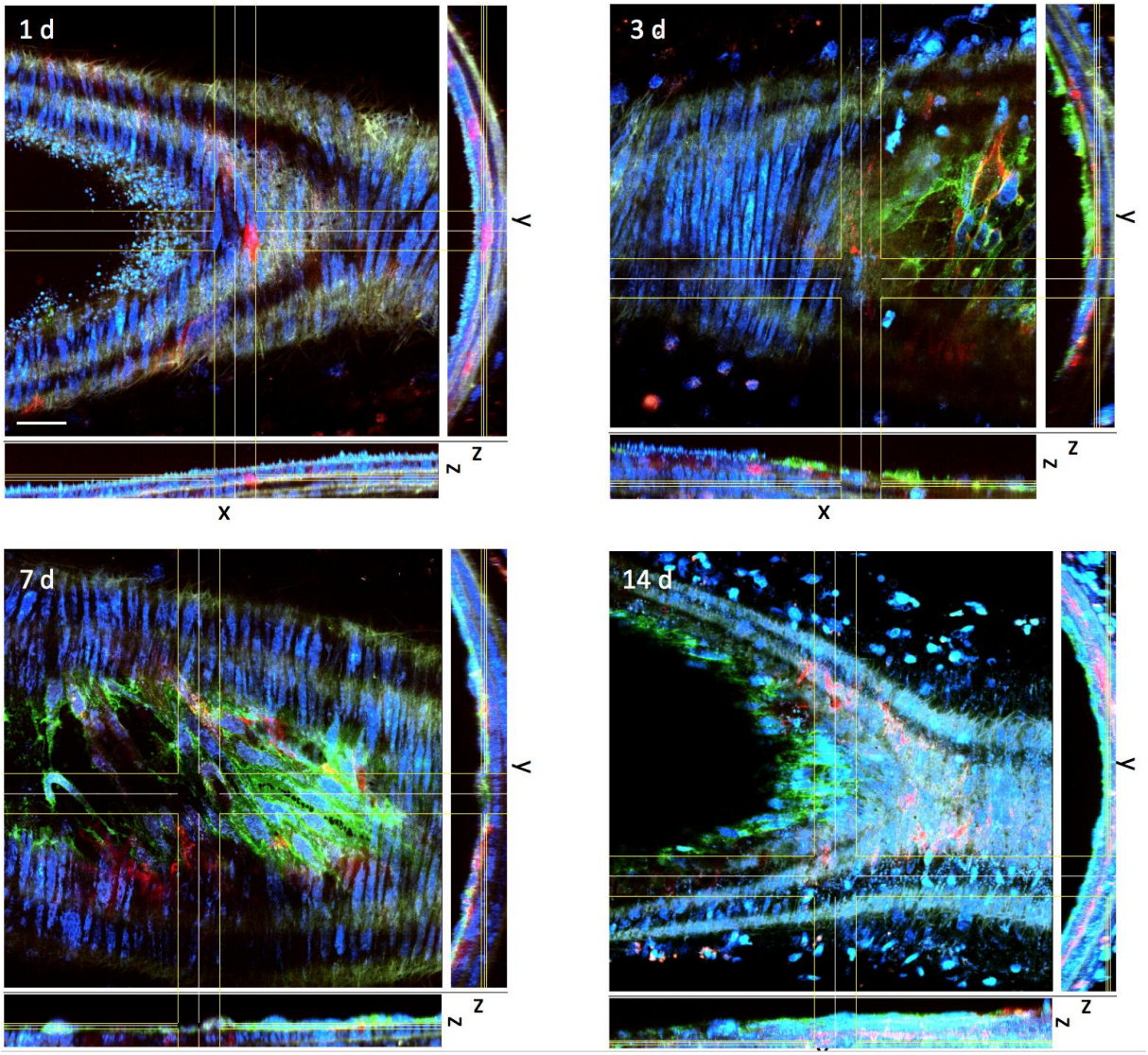

Supplemental Figure VIII: Raw image of ex vivo VCAM-1 and PECAM staining before 3D-rendering showing x-y, x-z and z-y slices of the carotid arteries (green = PECAM, red = VCAM-1, blue = nucleus, scale bar = 50 µm).

Supplemental Figure IX

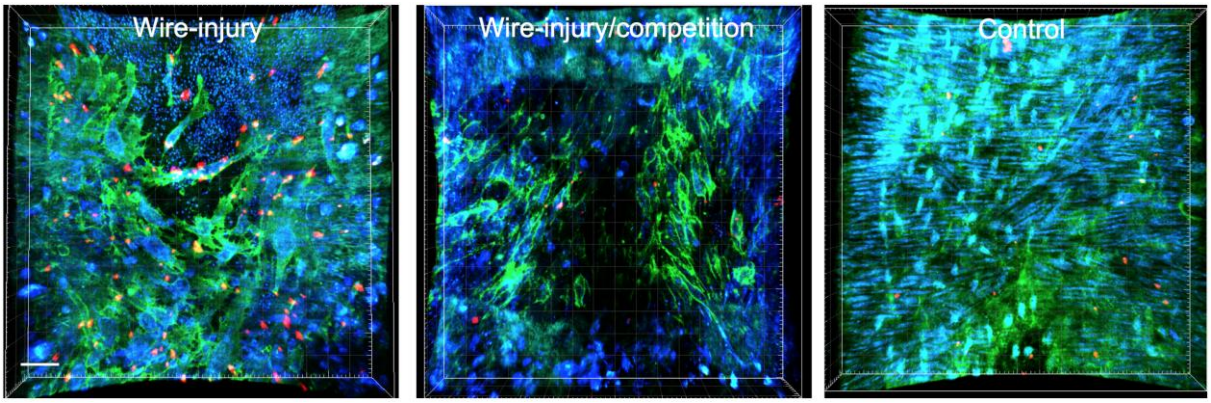

Supplemental Figure IX: Raw images of ex vivo binding assay using MB_{VCAM-1}. (green = PECAM, red = MB_{VCAM-1}, blue = nucleus, scale bar = 50 µm).

Supplemental Video

Supplemental Video I: *In vivo* TPLSM of wire-injured carotid arteries, 3 d post denudation. Five minutes after MB_{VCAM-1} injection, stationary MBs (red), highlighted by red circles, can be observed attached to the vessel wall (green). Due to respiratory motion, the focal plane drops in and out of focus.

Supplemental References:

1. Ilan N, Madri JA. PECAM-1: old friend, new partners. *Curr Opin Cell Biol.* 2003;15:515-524.
2. Davies MJ, Gordon JL, Gearing AJ, et al. The expression of the adhesion molecules ICAM-1, VCAM-1, PECAM, and E-selectin in human atherosclerosis. *J Pathol.* 1993;171:223-229.
3. Cai Q, Lanting L, Natarajan R. Interaction of monocytes with vascular smooth muscle cells regulates monocyte survival and differentiation through distinct pathways. *Arterioscler Thromb Vasc Biol*. 2004;24:2263-2270.
4. Wu Z, Curaj A, Fokong S, et al. Rhodamine-Loaded Intercellular Adhesion Molecule-1-targeted Microbubbles for Dual-Modality Imaging Under Controlled Shear Stresses. *Circ Cardiovasc Imaging*. 2013;6:974-981.
5. Simsekyilmaz S, Cabrera-Fuentes HA, Meiler S, et al. Role of extracellular RNA in atherosclerotic plaque formation in mice. *Circulation*. 2014;129:598-606.
6. Lindner V, Collins T. Expression of NF-kappa B and I kappa B-alpha by aortic endothelium in an arterial injury model. *Am J Pathol*. 1996;148:427-438.
7. Kennedy S, McPhaden AR, Wadsworth RM, Wainwright CL. Correlation of leukocyte adhesiveness, adhesion molecule expression and leukocyte-induced contraction following balloon angioplasty. *Br J Pharmacol.* 2000;130:95-103.
8. Schober A, Zernecke A, Liehn EA, et al. Crucial role of the CCL2/CCR2 axis in neointimal hyperplasia after arterial injury in hyperlipidemic mice involves early monocyte recruitment and CCL2 presentation on platelets. *Circ Res*. 2004;95:1125-1133.
9. Zeiffer U, Schober A, Lietz M, et al. Neointimal smooth muscle cells display a proinflammatory phenotype resulting in increased leukocyte recruitment mediated by P-selectin and chemokines. *Circ Res.* 2004;94:776-784.